Ramming et al., Tab. S1

Tab. S1. Characteristics of the *Shigella* and STEC AB_5 Shiga toxins

	Stx	Stx1	Stx2	Reference
Organism	*Shigella dysenteriae*	STEC	STEC	
Subtypes	1a	1a, 1c, 1d	2a-o	Scheutz et al., 2012 Yang et al., 2022
Protein sequence identity to Stx of *S. dysenteriae*	100 %	91 – 99 %*	~ 55 %*	Bergan et al., 2012
No. of amino acids		A1: 251 A2: 42	A1: 250 A2: 47	Li & Tumer, 2017
Active site in StxA1	Glu 167	Glu 167 covered by the A2 chain in the holotoxin (A1-A2)	Glu 166 open conformation in the holotoxin (A1-A2)	Yamasaki et al., 1991 Steyert et al., 2012 Jackson, 1990
Bacterial growth media and Stx production	n.k.	Culture media affect bacterial growth and concentration of Stx in supernatants		Rocha & Piazza, 2007
Activity of StxA1 on SRL RNA	n.k.	k_{cat} = 21.5 min^{-1}; lower compared to Stx2A1	k_{cat} = 62.6 min^{-1}; higher compared to Stx1A1	Basu et al., 2015
Optimal pH for activity	n.k.	*in vitro*: acidic pH (pH 4.5)		Basu et al., 2015
Activity and temperature	Activity loss ≥ 65°C	Activity loss ≥ 65°C	Activity loss ≥ 85°C	Chan & Ng, 2016

* Sequence identities of all Stx subtypes are summarized in Bergan *et al.,* 2012; n.k., not known

Ramming et al., Fig. S1

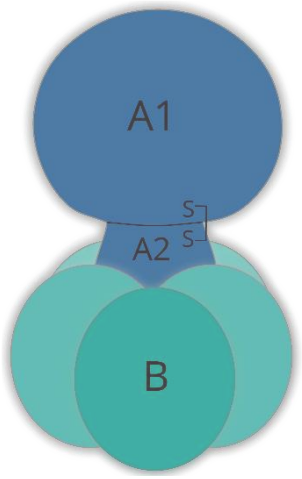

Sub-unit	MW [kDa]	No. of amino acids (without signal peptide)		Function	Reference
		Stx1	Stx2		
A	32	293	297	A1 and A2 connected by disulfide bridge after cleavage by furin	Gyles et al., 1988 Scheutz et al., 2012
A1	27.5	251	250	Enzymatic activity, 28S rRNA *N*-glycosidase activity	Scheutz et al., 2012
A2	4.5	42	47	Indispensable for holotoxin structure	Menge, 2020
B	7.7	69	68–70	Binding to Gb3/CD77 receptor	Takeda et al., 1993

Fig. S1. Structure of the STEC AB5 toxin Shiga toxin (Bergan et al., 2012) and characteristics of Stx1 and Stx2 A and B subunits.

Ramming et al., Fig. S2

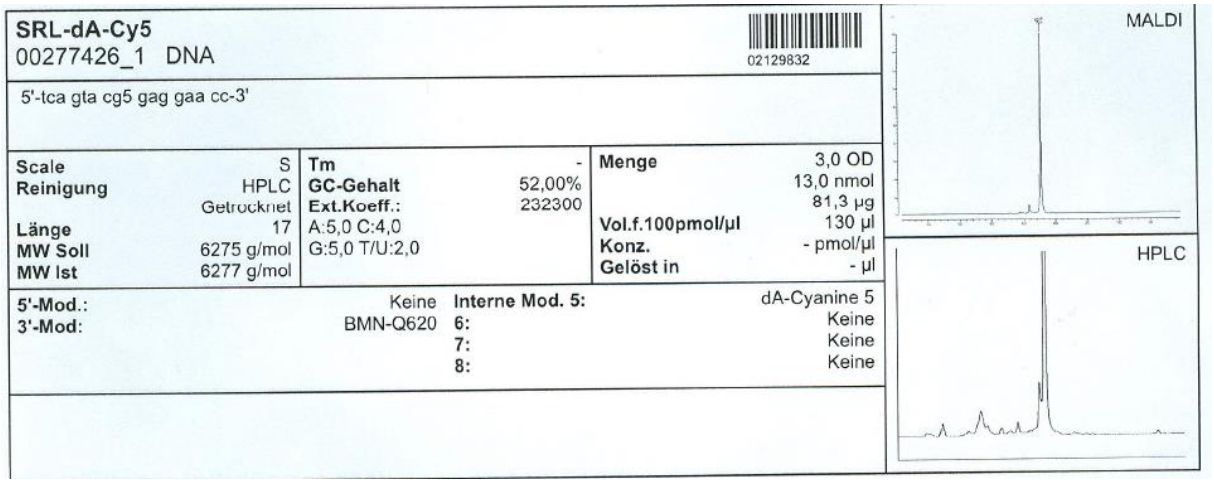

Fig. S2. Quality control analysis report of StxSense 1 (biomers.net).

Ramming et al., Fig. S3

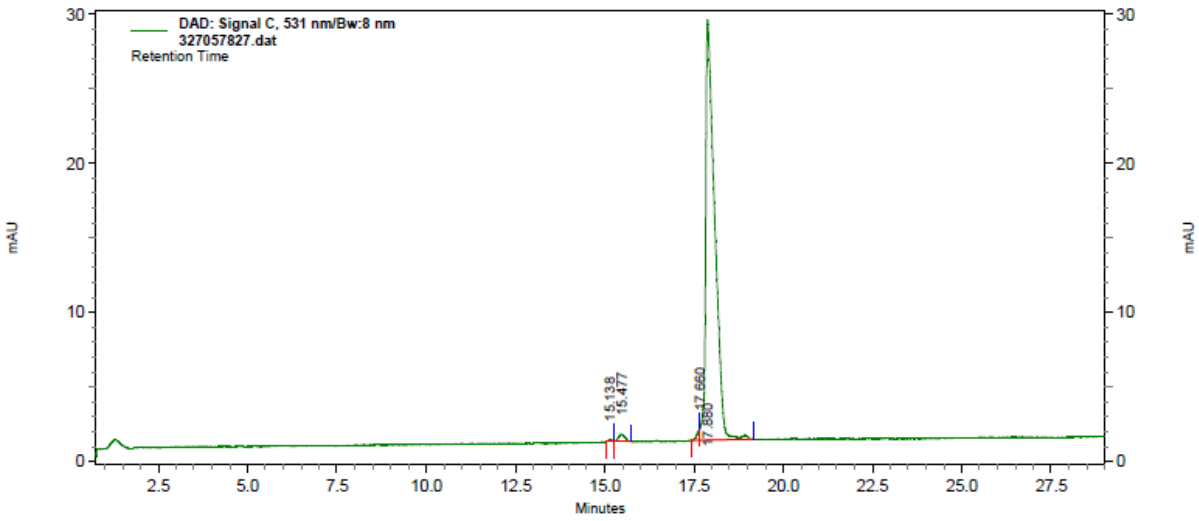

DAD: Signal C, 531 nm/Bw:8 nm Results

Peak #	Time	Height	Area	Area Percent
1	15.14	293	2387	0.2
2	15.48	1108	14277	1.3
3	17.66	1460	7702	0.7
4	17.88	59110	1033939	97.7
Totals		61971	1058305	100.0

Fig. S3. Quality control analysis report of StxSense 2 (integrated DNA Technologies, idt).

Ramming et al., Fig. S4

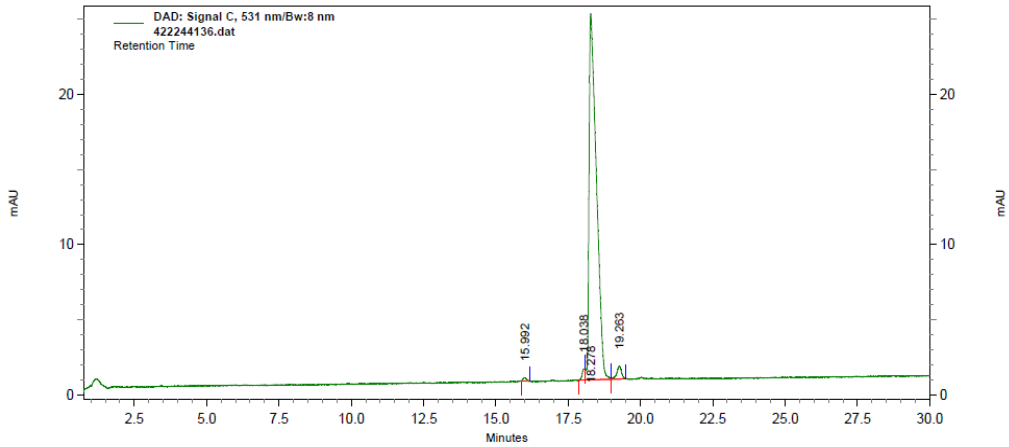

DAD: Signal C, 531 nm/Bw:8 nm Results

Peak #	Time	Height	Area	Area Percent
1	15.99	483	4016	0.4
2	18.04	1597	10996	1.2
3	18.28	51150	900948	96.2
4	19.26	1827	20544	2.2
Totals		55057	936504	100.0

Fig. S4. Quality control analysis report of StxSense 3 (integrated DNA Technologies, idt).

Ramming et al., Fig. S5

Integrated DNA Technologies Page 1 of 1

Analytical OligoPro CE Report

Sample ID: 233071385-21 SS HPLC A2 55887
Instrument: Oligo Pro (Offline) Operator: HTA
Acquired: 8/22/2022 5:55:00 AM Reviewed: 8/22/2022 7:48:16 AM

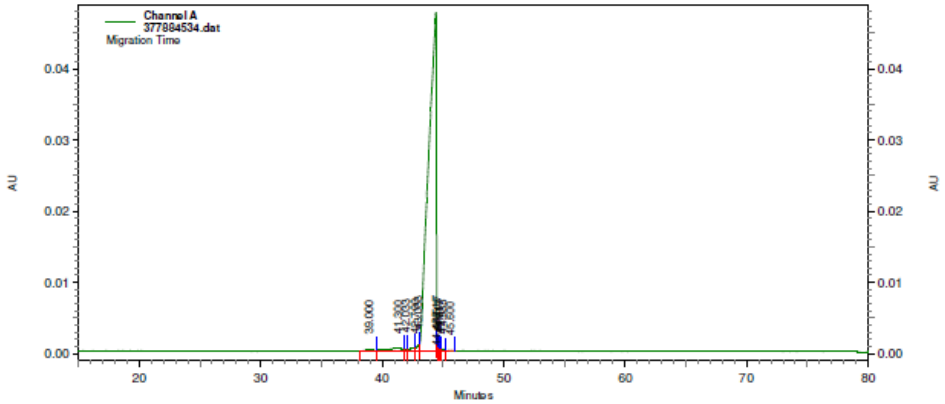

Channel A Results

Peak #	Time	Height	Corrected Area	Corrected Area Percent
1	39.00	145	160	0.4
2	41.30	372	757	1.7
3	42.03	284	92	0.2
4	42.70	456	294	0.7
5	43.03	821	258	0.6
6	44.43	47506	42884	95.9
7	44.52	879	50	0.1
8	44.62	433	45	0.1
9	44.72	292	43	0.1
10	44.98	269	86	0.2
11	45.60	70	31	0.1
Totals		51527	44700	100.0

Fig. S5. Quality control analysis report of StxSense 4 (integrated DNA Technologies, idt).

Ramming et al., Fig. S6: SRL substrates (belongs to Fig. 2)

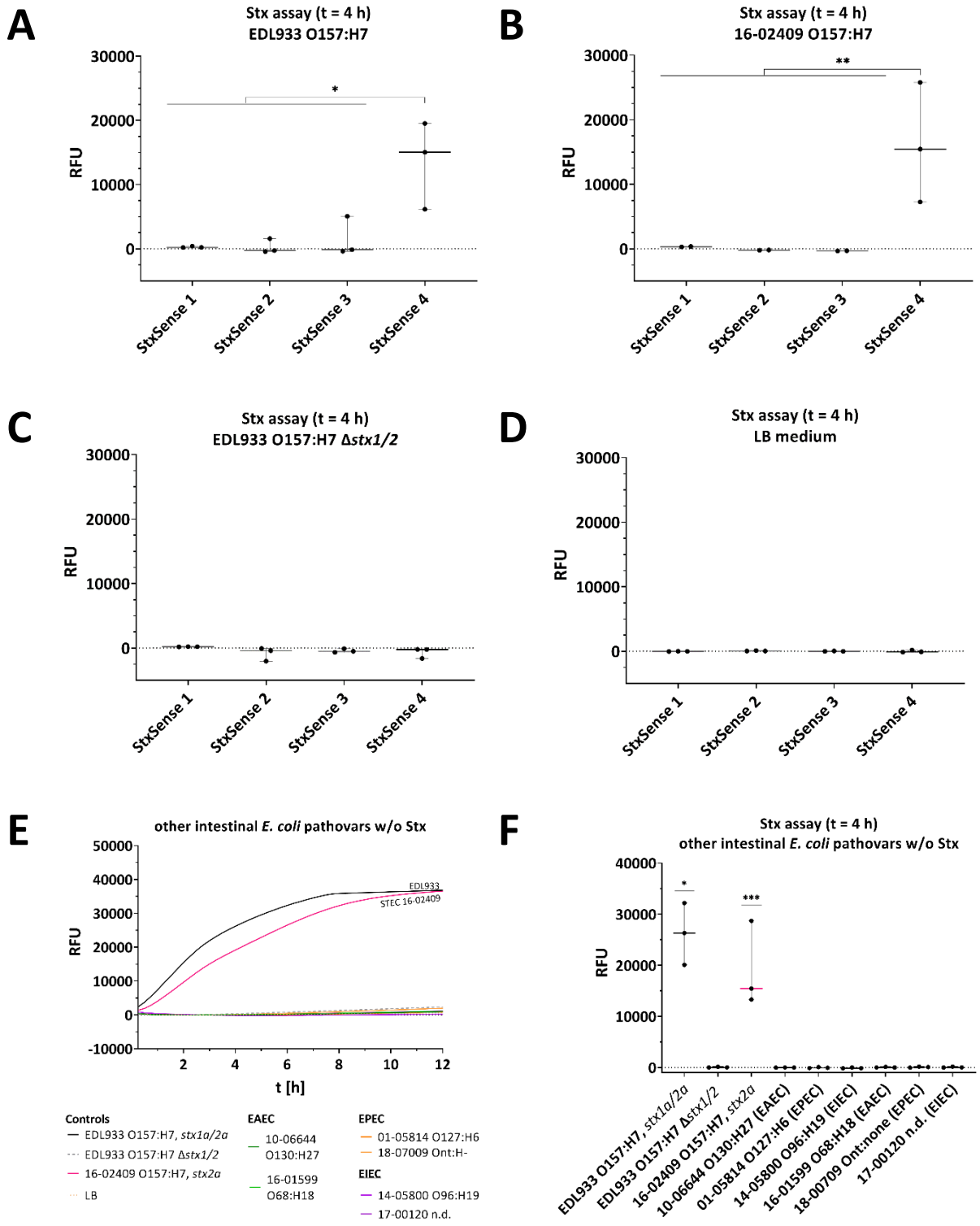

Ramming et al., Fig. S6 continued

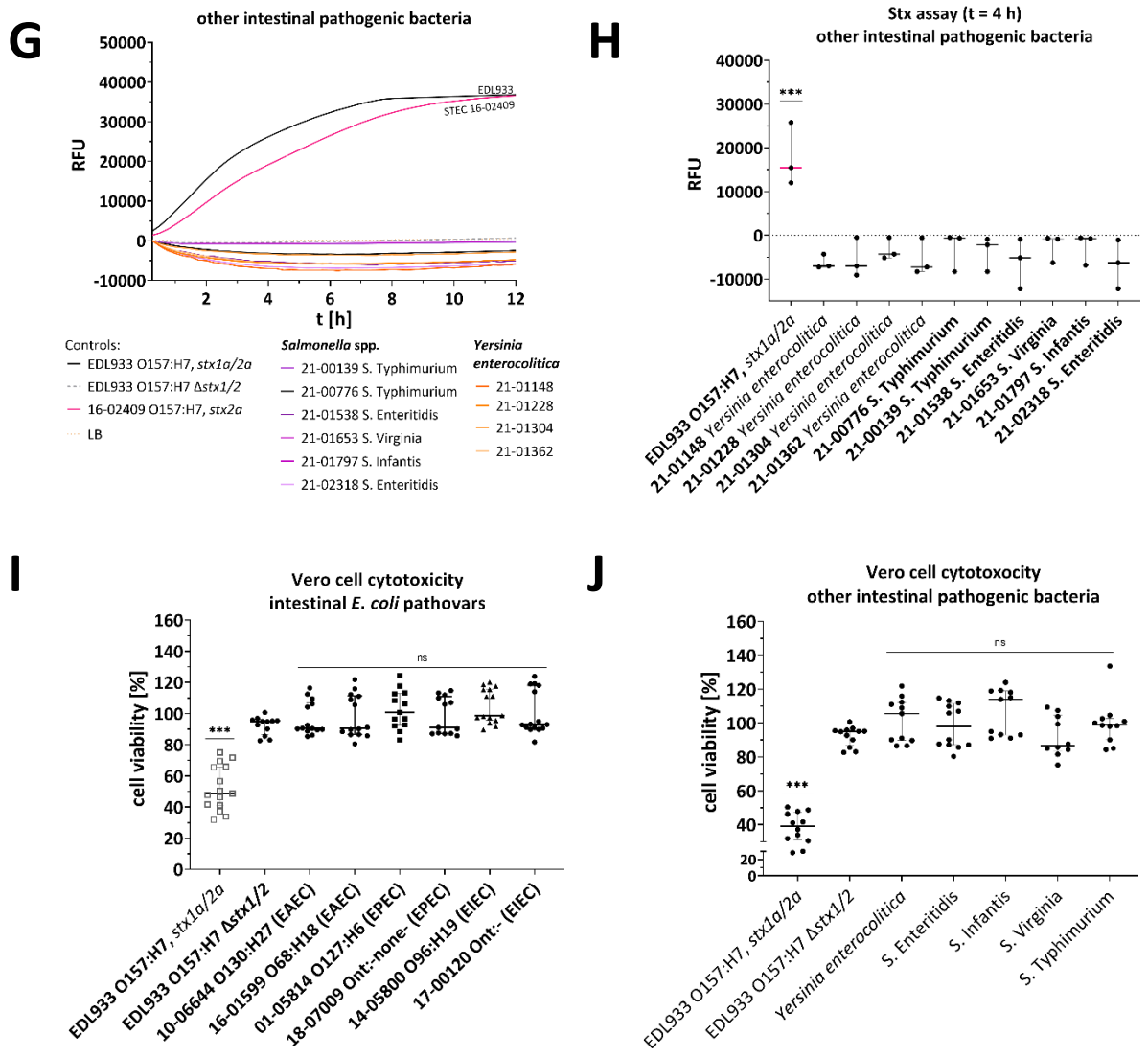

Fig. S6. Statistics of the Stx enzyme activity assay for STEC and controls. Statistics of the Vero cell cytotoxicity and Stx enzyme activity assay for other intestinal pathogenic bacteria producing no Stx. Detected fluorescence as a marker of substrate hydrolysis by Stx from different culture supernatants after 4 h incubation of **(A)** EDL933 O157:H7, *stx1a/2a*; **(B)** 16-02409 O157:H7, *stx2a*, **(C)** EDL933 O157:H7 Δ*stx1/2*, and **(D)** LB using the four SRL substrates. Data refer to the data shown in Fig. 2. Other intestinal *E. coli* pathovars: **(E and F)** Stx enzymatic activity assay for culture supernatants for up to 12 h (E) or for 4 h (F) and **(I)** Vero cell cytotoxicity assay. Other intestinal pathogenic bacteria: **(G and H)** Stx enzymatic activity assay for culture supernatants for up to 12 h (H) or for 4 h (I) and **(J)** Vero cell cytotoxicity assay. For Vero cell cytotoxicity assay, cell viability of Vero cells was analyzed using MTT assay after inoculation with diluted bacterial culture supernatants (1:400) for 48 h**.** For statistics of Stx enzymatic activity assay, RFU at 4 h reaction time and 44 °C are shown. The results represent the medians of triplicate samples (n = 3) and are representative of three independent experiments. Error bars represent standard deviation. Statistical analysis was performed by unpaired, double-sided t test (A-D, F, H), Mann-Whitney test (I and J) (*, $p < 0.05$; **, $p < 0.01$; ***, $p < 0.001$), with results compared to those of EDL933 O157:H7 Δ*stx1/2*. RFU, Relative Fluorescent Unit.

Ramming et al., Fig. S7: assay conditions

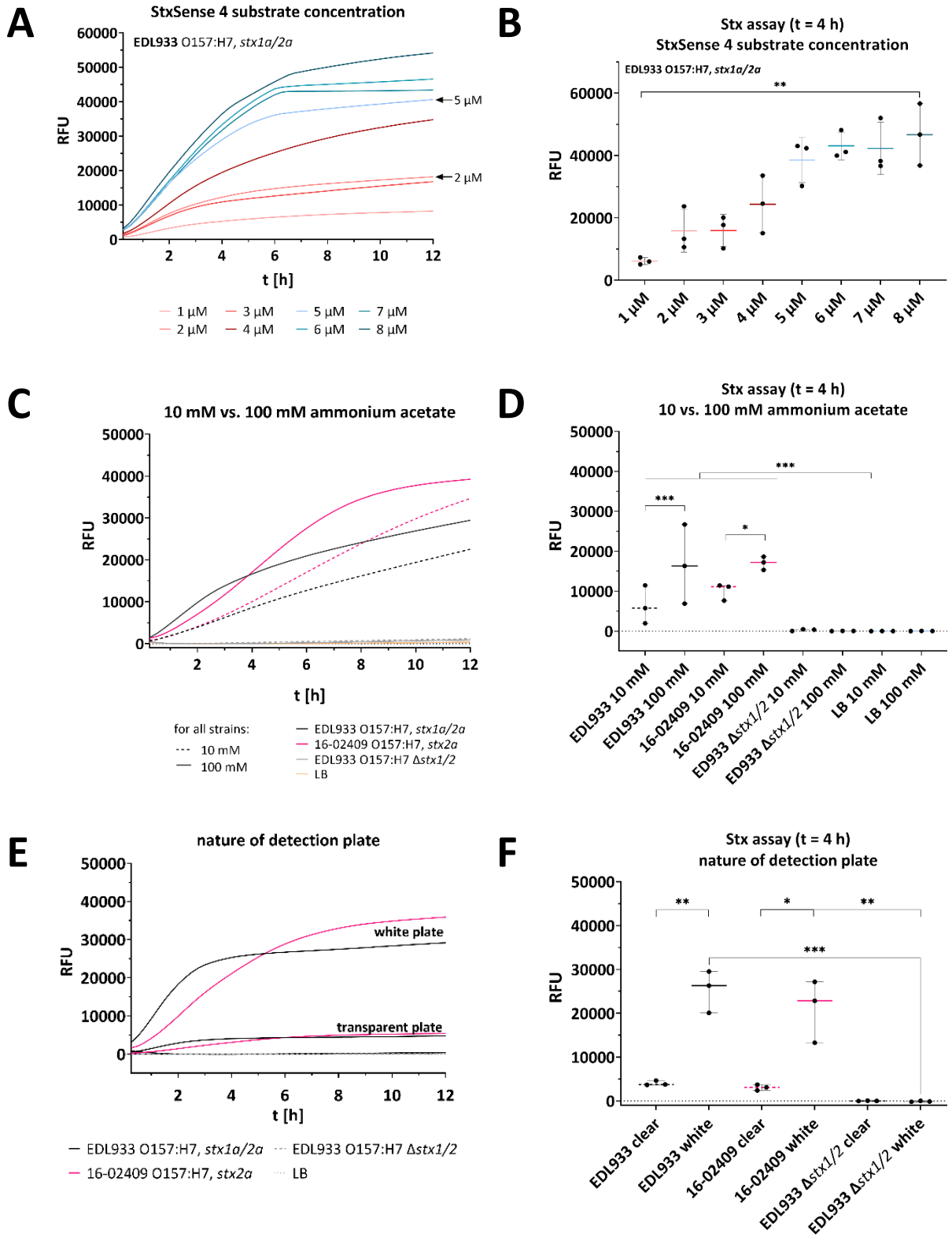

Ramming et al., Fig. S7 continued

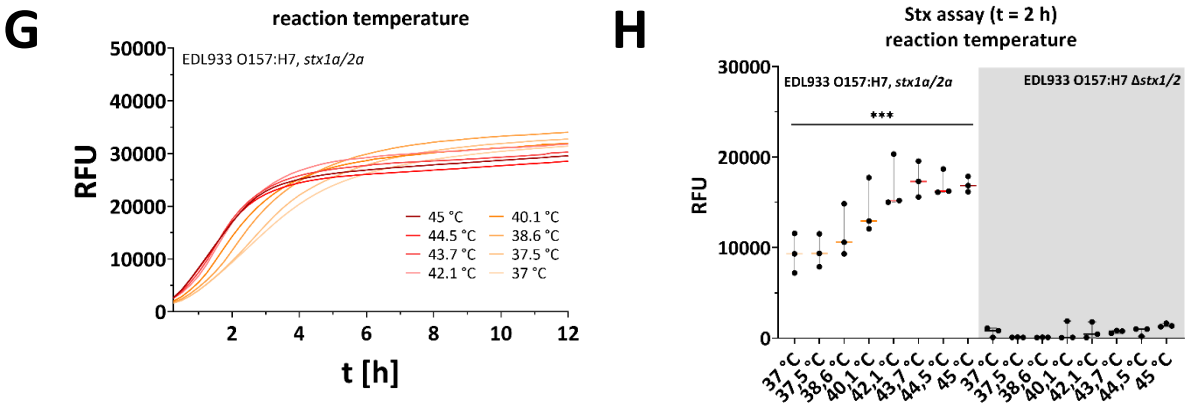

Fig. S7. Optimal assay conditions for Stx detection in culture supernatants. Detected fluorescence as a marker of substrate hydrolysis by Stx from positive control EDL933 O157:H7, *stx1a/2a* and/or test strain STEC 16-02409 O157:H7, *stx2a*, and negative control EDL933 O157:H7 Δ*stx1/2*. **(A and B)** Optimal fluorescence readout for Stx was achieved using SRL substrate StxSense 4 concentrations from 2 µM in 100 mM ammonium acetate. **(C and D)** 100 mM ammonium acetate yielded in higher fluorescence signals *stx2a*-producing strain compared to 10 mM ammonium acetate. **(E and F)** Using a white 96 well plate instead of a clear plate was essential for fluorescence detection of Stx-positive samples. **(G and H)** Reaction temperatures above 43.7 °C were optimal Stx detection. Reaction conditions for (A, B, E, F) were 44 °C, 100 mM ammonium acetate, 2 µM StxSense 4. The results represent the medians of triplicate samples (n = 3) and are representative of three independent experiments. Error bars represent standard deviation. Statistical analysis was performed by Mann-Whitney test for non-normally distributed samples (B, H) and unpaired, double-sided t test (D, F) (*, $p < 0.05$; **, $p < 0.01$; ***, $p < 0.001$), with results compared to those of EDL933 O157:H7 Δ*stx1/2* (negative control; -- [grey dashed lines]). RFU, relative fluorescence units; t [h], time [hours].

Ramming et al., Fig. S8: Stx-producing strains (belongs to Fig. 4)

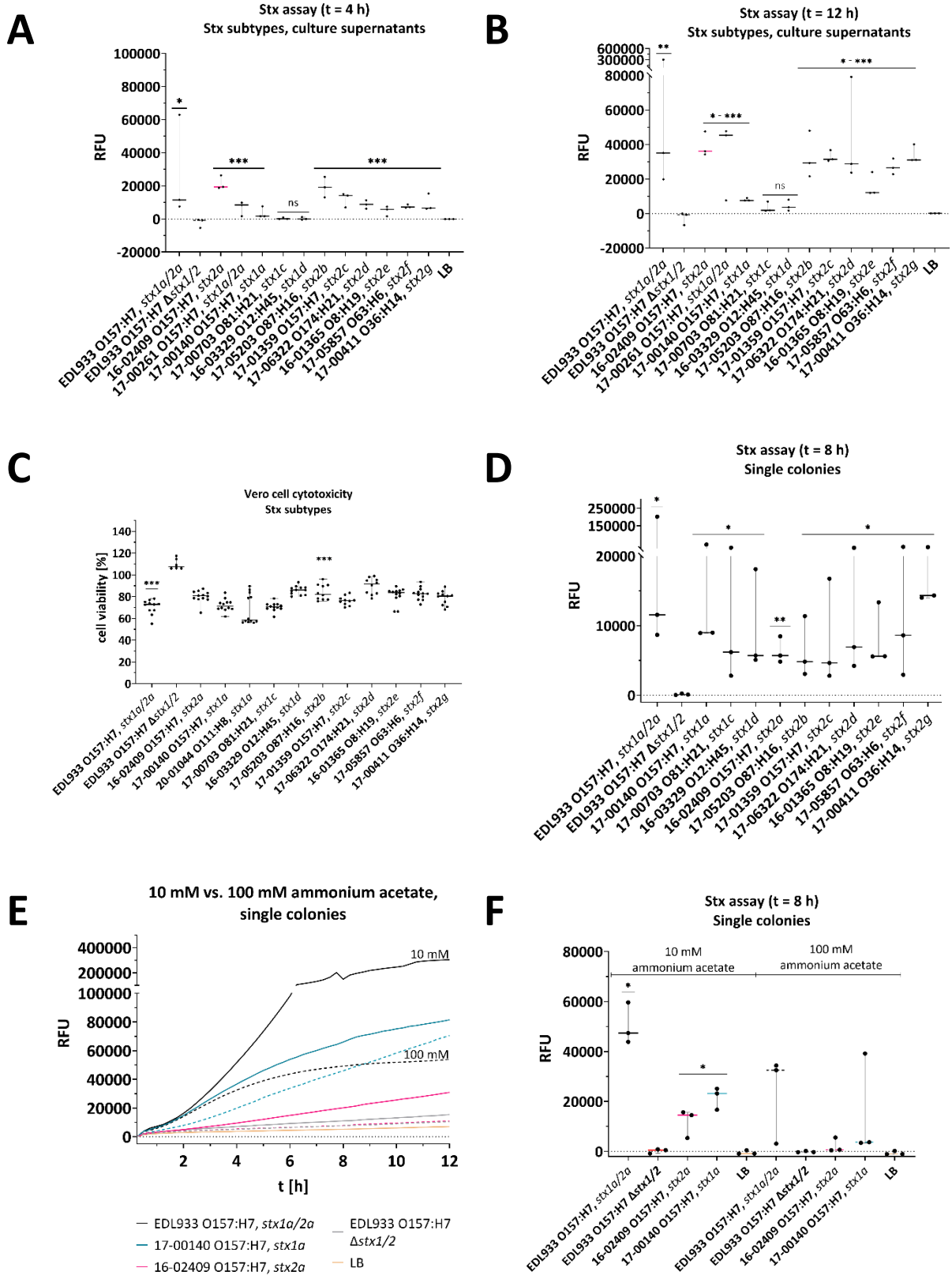

Ramming et al., Fig. S8 continued

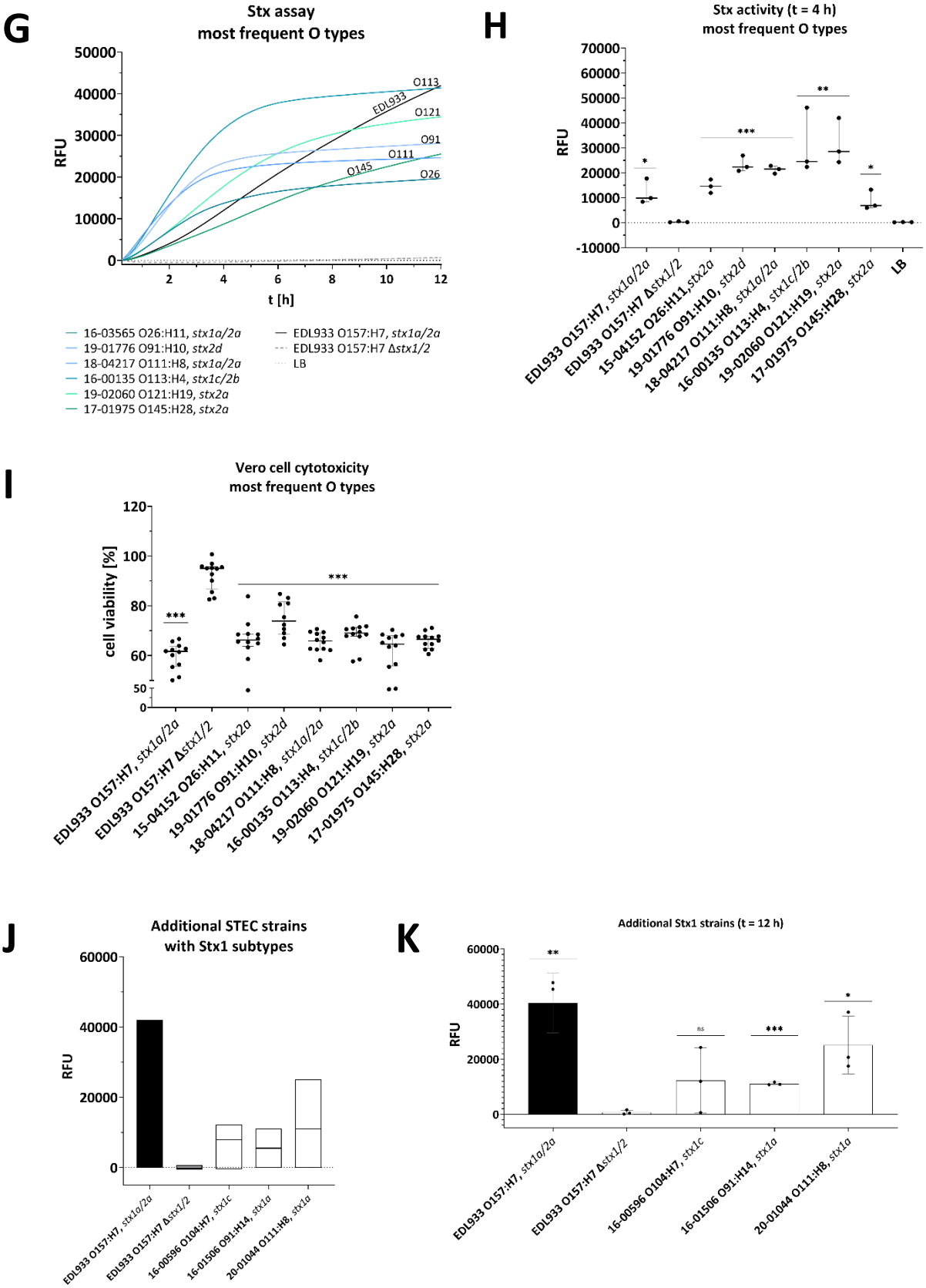

Ramming et al., Fig. S8 continued (2)

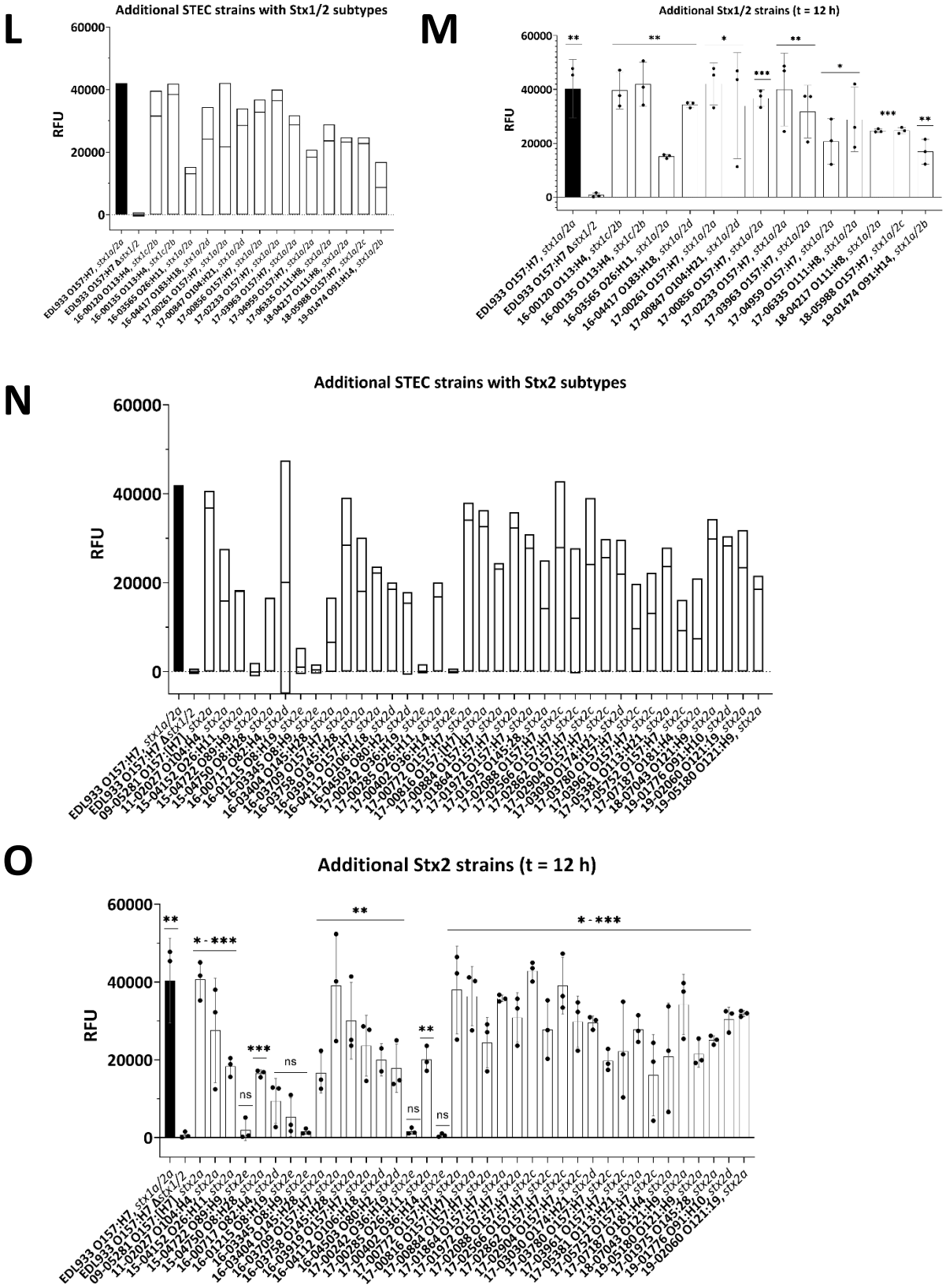

Ramming et al., Fig. S8 continued (3)

P

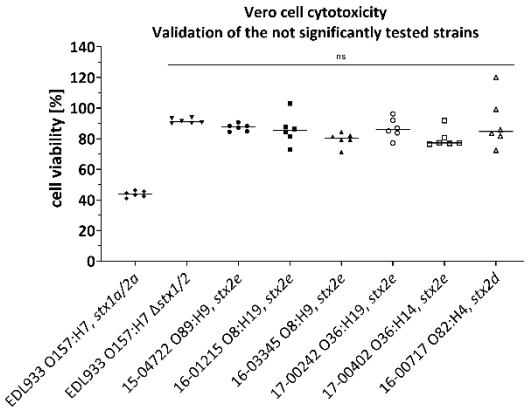

Fig. S8. Statistics of Vero cell cytotoxicity assay and Stx activity assay for Stx1 and Stx2 subtypes (see Fig. 4A). (A, B, D-H, J-O) Detected fluorescence of Stx activity from **(A and B)** culture supernatants of STEC strains covering Stx1a-Stx1d and Stx2a-2g at (A) 4 h and (B) 12 h; **(D)** single colonies of STEC strains covering Stx1a-Stx1d and Stx2a-2g, **(E and F)** single colonies of STEC strains and influence of 10 mM vs. 100 mM ammonium acetate, **(G and H)** most frequent serotypes; **(J to O)** Detected fluorescence of culture supernatants of different STEC strains comprising **(J and K)** Stx1, **(L and M)** Stx1/2, **(N and O)** Stx2, with positive control EDL933 O157:H7, *stx1a/2a* (black filled bar), and negative control EDL933 O157:H7 Δ*stx1/2* (grey filled bar) as floating bars (min to max RFU) with line at the median RFU over 12 h and statistics. (J to O) were performed within the same analysis. Shown are the RFU of culture supernatants at 4 h reaction time in 100 mM ammonium acetate, if not stated otherwise, 2 µM StxSense 4, 44 °C, white reaction plate. **(C, I and P)** Cell viability of Vero cells was analyzed using MTT assay after inoculation with diluted bacterial culture supernatants (1:400) for 48 h: **(C)** STEC strains comprising different Stx subtypes, **(I)** most frequent serotypes. Data refer to the data shown in Fig. 4, **(P)** Verification of STEC strains not significantly tested within the STEC detection assay. The results are medians of triplicate samples (n = 3) of three independent experiments. Error bars represent standard deviation. Statistical analysis was performed by Mann-Whitney test (A, B, D-F, H, K, M, O) and unpaired, double-sided t test (C, I) (*, $p < 0.05$; **, $p < 0.01$; ***, $p < 0.001$), with results compared to those of EDL933 O157:H7 Δ*stx1/2*. RFU, Relative Fluorescent Unit; ns, not significant.

Ramming et al., Fig. S9: *Shigella*

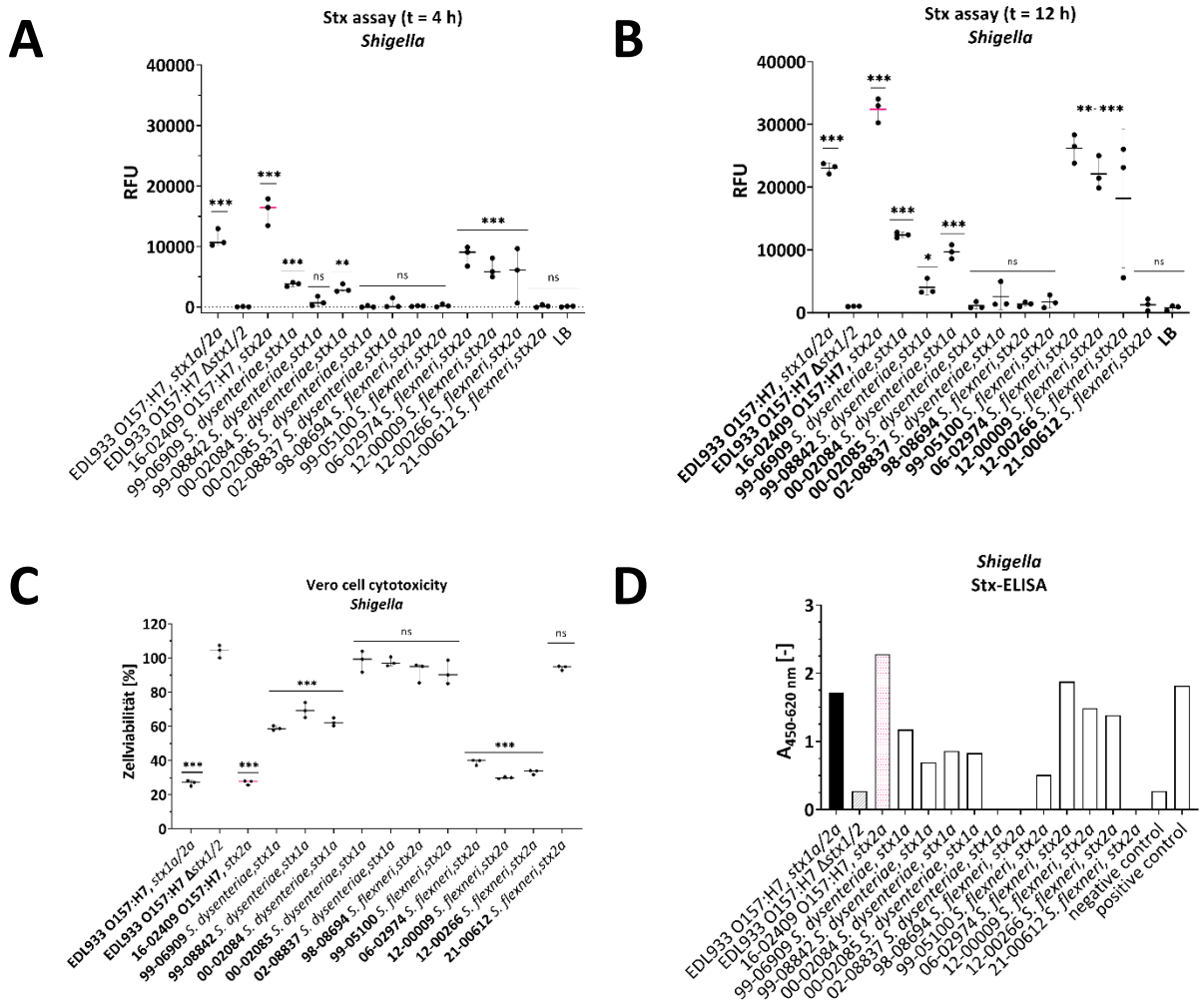

Fig. S9. Statistics of Vero cell cytotoxicity assay and Stx activity assay for different *Shigella* strains. (A and B) Detected fluorescence of culture supernatants of different *Shigella* spp. strains and positive control EDL933 O157:H7, *stx1a/2a*, STEC strain 16-02409 O157:H7, *stx2a* and negative control EDL933 O157:H7 Δ*stx1/2* at (A) 4h and (B) 12 h. The assay was performed using 100 mM ammonium acetate, 2 µM StxSense 4, 44 °C. **(C)** Cell viability of Vero cells was analyzed using MTT assay after inoculation with diluted bacterial culture supernatants (1:400) for 48 h. **(D)** Commercial Stx ELISA (R-Biopharm AG, Darmstadt, Germany) of culture supernatant (OD_{600} of 3.0) from different *Shigella* strains detecting Stx1 and Stx2 (n = 1). All other results are medians of triplicate samples (n = 3) of three independent experiments. Error bars represent standard deviation. Statistical analysis was performed by Mann-Whitney test (A) and unpaired, double-sided t test (B) (*, $p < 0.05$; **, $p < 0.01$; ***, $p < 0.001$) with results compared to those of EDL933 O157:H7 Δ*stx1/2*. RFU, Relative Fluorescent Unit; ns, not significant.

Table S2: STEC strains used in the study (Ramming et al., xxx).

In total, 65 STEC strains were analyzed for Stx activity. The determined genome sequences were uploaded to the European Nucleotide Archive under the study Acc. No. PRJEB32361 (Lang et al., 2019; Lang et al., 2023). The STEC serotype was determined using Whole Genome Analysis, classical serotyping or PCR-based serotyping (Scheutz et al., 2012; Lang et al., 2019). *eaeA* presence was determined using Whole Genome Analysis or PCR-based serotyping (Schmidt et al., 1993; Lang et al., 2019). n.d., not determined; +, positive analysis test result; -, negative analysis test result; ns, not significant.

	Strain No.	Year of isolation	O group	H type	MLST sequence type	Accession No.	stx1 subtype	stx2 subtype	*eaeA*	Reference	FRET assay supernatant	where to find?
1	**EDL933**	2001	157	7	11	GCF_000732965.1	stx1a	stx2a	+	Perna et al., 2001	+	pos control
2	**EDL933 Δ*stx1/2***	2007	157	7	n.d.	-	-	-	+	Gobert et al., 2007	-	neg control
3	**09-05281**	2009	157	-/[7]	n.d.	n.d.	-	stx2a	+	This study	+	Fig. S8N
4	**11-02027**	2011	104	4	678	SAMN03168461	-	stx2a	-	Frank et al., 2011	+	Fig. S8N
5	**15-04152**	2015	26	11	29	ERS3396064 (SAMEA5591849)	-	stx2a	+	Lang et al., 2019	+	Fig. S8N
6	**15-04722**	2015	89	9	10	ERS3396066 (SAMEA5591851)	-	stx2e	-	Lang et al., 2019	n.s.	Fig. S8N
7	**15-04750**	2015	8	28	162	ERS3396067 (SAMEA5591852)	-	stx2e	-	Lang et al., 2019	+	Fig. S8N
8	**16-00120**	2016	113	4	10	ERS3396073 (SAMEA5591858)	stx1c	stx2b	-	Lang et al., 2019	+	Fig. S8L
9	**16-00135**	2016	113	4	10	ERS3396074 (SAMEA5591859)	stx1c	stx2b	-	Lang et al., 2019	+	Fig. S8G
10	**16-00596**	2016	104	7	1817	ERS3396083 (SAMEA5591868)	stx1c	-	-	Lang et al., 2019	+	Fig. S8J
11	**16-00717**	2016	82	4	10	ERS3396090 (SAMEA5591875)	-	stx2d	-	Lang et al., 2019	n.s.	Fig. S8N
12	**16-01215**	2016	8	19	88	ERS3396098 (SAMEA5591883)	-	stx2e	-	Lang et al., 2019	n.s.	Fig. S8N
13	**16-01365**	2016	8	19	201	ERS3396100 (SAMEA5591885)	-	stx2e	-	Lang et al., 2019	+	Fig. 4A/B
14	**16-01506**	2016	91	14	33	ERS3396103 (SAMEA5591888)	stx1a	-	-	Lang et al., 2019	+	Fig. S8J
15	**16-02409**	2016	157	7	11	ERS3396113 (SAMEA5591898)	-	stx2a	+	Lang et al., 2019	+	Fig. 2, 4C
16	**16-03329**	2016	12	45	n.d.	ERS3396123 (SAMEA5591908)	stx1d	-	-	Lang et al., 2019	+	Fig. 4A/B
17	**16-03345**	2016	8	9	23	ERS3396125 (SAMEA5591910)	-	stx2e	-	Lang et al., 2019	n.s.	Fig. S8N
18	**16-03404**	2016	145	28	32	ERS3396126 (SAMEA5591911)	-	stx2a	+	Lang et al., 2019	+	Fig. S8N
19	**16-03565**	2016	26	11	21	ERS3396129 (SAMEA5591914)	stx1a	stx2a	+	Lang et al., 2019	+	Fig. S8G
20	**16-03709**	2016	157	7	11	ERS3396134 (SAMEA5591919)	-	stx2a	+	Lang et al., 2019	+	Fig. S8N
21	**16-03758**	2016	145	28	32	ERS3396135 (SAMEA5591920)	-	stx2a	+	Lang et al., 2019	+	Fig. S8N
22	**16-03919**	2016	157	7	11	ERS3396136 (SAMEA5591921)	-	stx2a	+	Lang et al., 2019	+	Fig. S8N
23	**16-04112**	2016	106	18	663	ERS3396140 (SAMEA5591925)	-	stx2d	-	Lang et al., 2019	+	Fig. S8N
24	**16-04417**	2016	183	18	657	ERS3396151 (SAMEA5591936)	stx1a	stx2d	-	Lang et al., 2019	+	Fig. S8L
25	**16-04503**	2016	80	2	301	ERS3396152 (SAMEA5591937)	-	stx2d	+	Lang et al., 2019	+	Fig. S8N
26	**17-00140-1**	2017	157	7	11	ERS3396169 (SAMEA5591954)	stx1a	-	+	Lang et al., 2019	+	Fig. 4A/B
27	**17-00242**	2017	36	19	10	ERS3396170 (SAMEA5591955)	-	stx2e	-	Lang et al., 2019	n.s.	Fig. S8L
28	**17-00261**	2017	157	7	11	ERS3396171 (SAMEA5591956)	stx1a	stx2a	+	Lang et al., 2019	+	Fig. 4A/B
29	**17-00285**	2017	26	11	29	ERS3396172 (SAMEA5591957)	-	stx2a	+	Lang et al., 2019	+	Fig. S8L
30	**17-00402**	2017	36	14	1176	ERS3396173 (SAMEA5591958)	-	stx2e	-	Lang et al., 2019	n.s.	Fig. S8L
31	**17-00411**	2017	36	14	1176	ERS3396174 (SAMEA5591959)	-	stx2g	-	Lang et al., 2019	+	Fig. 4A/B
32	**17-00703**	2017	81	21	737	ERS3396178 (SAMEA5591963)	stx1c	-	-	Lang et al., 2019	+	Fig. 4A/B
33	**17-00772**	2017	157	7	11	ERS3396179 (SAMEA5591964)	-	stx2a	+	Lang et al., 2019	+	Fig. S8N
34	**17-00816**	2017	157	-/[7]	n.d.	n.d.	-	stx2a	+	This study	+	Fig. S8N
35	**17-00847**	2017	104	21	672	ERS3396182 (SAMEA5591967)	stx1a	stx2d	-	Lang et al., 2019	+	Fig. S8L
36	**17-00856**	2017	157	7	11	ERS3396183 (SAMEA5591968)	stx1a	stx2a	+	Lang et al., 2019	+	Fig. S8L
37	**17-00884**	2017	157	7	11	ERS3396185 (SAMEA5591970)	-	stx2a	+	Lang et al., 2019	+	Fig. S8N
38	**17-01359**	2017	157	7	11	ERS3396196 (SAMEA5591981)	-	stx2c	+	Lang et al., 2019	+	Fig. 4A/B
39	**17-01864**	2017	157	7	11	ERS3396199 (SAMEA5591984)	-	stx2a	+	Lang et al., 2019	+	Fig. S8N
40	**17-01972**	2017	157	7	587	ERS3396200 (SAMEA5591985)	-	stx2a	+	Lang et al., 2019	+	Fig. S8N
41	**17-01975**	2017	145	28	32	ERS3396201 (SAMEA5591986)	-	stx2a	+	Lang et al., 2019	+	Fig. S8G
42	**17-02088**	2017	157	7	1804	ERS3396202 (SAMEA5591987)	-	stx2c	+	Lang et al., 2019	+	Fig. S8N
43	**17-02233**	2017	157	7	11	ERS3396203 (SAMEA5591988)	stx1a	stx2a	+	Lang et al., 2019	+	Fig. S8L
44	**17-02566**	2017	157	7	11	ERS3396204 (SAMEA5591989)	-	stx2c	+	Lang et al., 2019	+	Fig. S8N
45	**17-02862**	2017	157	7	11	ERS3396210 (SAMEA5591995)	-	stx2c	+	Lang et al., 2019	+	Fig. S8N
46	**17-02904**	2017	157	7	n.d.	n.d.	-	stx2c	+	This study	+	Fig. S8N
47	**17-03030**	2017	174	21	677	ERS3396212 (SAMEA5591997)	-	stx2d	-	Lang et al., 2019	+	Fig. S8N
48	**17-03780**	2017	157	7	11	ERS3396215 (SAMEA5592000)	-	stx2c	+	Lang et al., 2019	+	Fig. S8N
49	**17-03961**	2017	157	7	11	ERS3396218 (SAMEA5592003)	-	stx2c	+	Lang et al., 2019	+	Fig. S8N
50	**17-03963**	2017	157	7	11	ERS3396219 (SAMEA5592004)	stx1a	stx2a	+	Lang et al., 2019	+	Fig. S8L
51	**17-04959**	2017	157	7	11	ERS3396225 (SAMEA5592010)	stx1a	stx2a	+	Lang et al., 2019	+	Fig. S8L
52	**17-05203**	2017	87	16	2101	ERS3396229 (SAMEA5592014)	-	stx2b	-	Lang et al., 2019	+	Fig. 4A/B
53	**17-05381**	2017	113	21	223	ERS3396236 (SAMEA5592021)	-	stx2a	-	Lang et al., 2019	+	Fig. S8N
54	**17-05752**	2017	157	7	11	ERS3396247 (SAMEA5592032)	-	stx2c	+	Lang et al., 2019	+	Fig. S8N
55	**17-05857**	2017	63	6	583	ERS3396253 (SAMEA5592038)	-	stx2f	+	Lang et al., 2019	+	Fig. 4A/B
56	**17-06322**	2017	174	21	677	ERS3396266 (SAMEA5592051)	-	stx2d	-	Lang et al., 2019	+	Fig. 4A/B
57	**17-06335**	2017	111	8	16	ERS3396269 (SAMEA5592054)	stx1a	stx2a	+	Lang et al., 2019	+	Fig. S8L
58	**17-07187**	2017	181	4	n.d.	n.d.	-	stx2a	-	Lang et al., 2023	+	Fig. S8N
59	**18-04217**	2018	111	8	n.d.	n.d.	stx1a	stx2a	+	This study	+	Fig. S8G
60	**18-05988**	2018	157	7	n.d.	n.d.	stx1a	stx2c	+	This study	+	Fig. S8L
61	**18-07043**	2018	121	9	n.d.	n.d.	-	stx2a	+	This study	+	Fig. S8N
62	**19-01474**	2019	91	14	n.d.	n.d.	stx1a	stx2b	-	This study	+	Fig. S8L
63	**19-01776**	2019	91	10	n.d.	n.d.	-	stx2d	-	This study	+	Fig. S8G
64	**19-02060**	2019	121	19	n.d.	n.d.	-	stx2a	+	This study	+	Fig. S8G
65	**19-05180**	2019	121	19	n.d.	n.d.	-	stx2a	+	This study	+	Fig. S8N
66	**20-01044**	2020	111	8	n.d.	n.d.	stx1a	-	+	This study	+	Fig. S8J

References:

Perna, N., Plunkett, G., Burland, V. *et al.* Genome sequence of enterohaemorrhagic *Escherichia coli* O157:H7 . *Nature* **409**, 529–533 (**2001**). https:/

Gobert, A. P., Vareille, M., Glasser, A.-L., Hindré, T., de Sablet, T., & Martin, C. (**2007**). Shiga Toxin Produced by Enterohemorrhagic Escherichia coli Inhibits PI3K/NF-κB Signaling Pathway in Globotriaosylceramide-3-Negative Human Intestinal Epithelial Cells. *The Journal of Immunology*, *178*(12), 8168–8174.

Frank, C., Werber, D., Cramer, J. P., Askar, M., Faber, M., an der Heiden, M., Bernard, H., Fruth, A., Prager, R., Spode, A., Wadl, M., Zoufaly, A., Jordan, S., Kemper, M. J., Follin, P., Müller, L., King, L. A., Rosner, B., Buchholz, U., Krause, G. (**2011**). Epidemic Profile of Shiga-Toxin–Producing Escherichia coli O104:H4 Outbreak in Germany. *New England Journal of Medicine* , *365* (19), 1771–1780. https://doi.org/10.1056/nejmoa1106483

Lang, C., Hiller, M., Konrad, R., & Fruth, A. (**2019**). *Whole-Genome-Based Public Health Surveillance of LessCommon Shiga Toxin-ProducingEscherichia coliSerovars andUntypeable Strains Identifies Four Novel O Genotypes* . *September* , 1–12.

Lang, C., Fruth, A., Campbell, I. W., Jenkins, C., Smith, P., Weill, F.-X., Nübel, U., Grad, Y. H., & Flieger, A. (**2023**). O-antigen diversification masks identification of highly pathogenic STEC O104:H4-like 1 strains 2 3. *Microbiology Spectrum* . https://doi.org/10.1101/2022.09.15.508078

Table S3: Other intestinal *E. coli* pathovar strains without Stx used in the study (Ramming et al., xxx).

The *E. coli* pathovar serotype was determined using Whole Genome Analysis, classical serotyping or PCR-based serotyping (Scheutz et al., 2012; Lang et al., 2019). *eaeA* presence was determined using Whole Genome Analysis or PCR-based serotyping (Schmidt et al., 1993; Lang et al., 2019). n.d., not determined; +, positive analysis test result; -, negative analysis test result.

	Strain no.	Year of isolation	Pheno-typic O group	Pheno-typic H type	pathovar	*eaeA*	Reference	FRET assay supernatant	where to find?	Vero cell cytotoxicity assay	where to find?
1	**10-06644**	2010	130	27	EAEC	n.d.	This study	-	Fig. S6E, F	-	Fig. S6I
2	**16-01599-2**	2016	68	18	EAEC	-	This study	-	Fig. S6E, F	-	Fig. S6I
3	**01-05814**	2001	127	6	EPEC	+	This study	-	Fig. S6E, F	-	Fig. S6I
4	**18-07009-2**	2018	Ont	-	EPEC	+	This study	-	Fig. S6E, F	-	Fig. S6I
5	**18-07383-2**	2018	Ont	-	EPEC	+	This study	-	Fig. S6E, F	-	Fig. S6I
6	**14-05800-2**	2014	96	19	EIEC	n.d.	This study	-	Fig. S6E, F	-	Fig. S6I
7	**17-00120**	2017	n.d.	n.d.	EIEC	n.d.	This study	-	Fig. S6E, F	-	Fig. S6I

Table S4: *Yersinia* and *Salmonella* strains used in the study (Ramming et al., xxx).

The species or serovar was determined using Whole Genome Analysis, classical serotyping or PCR-based serotyping (Lang et al., 2019). +, positive analysis test result; -, negative analysis test result.

	Strain no.	Year of isolation	Species or serovar	Stx1 subtype	Stx2 subtype	Reference	FRET assay supernatant	where to find?	Vero cell cytotoxicity assay	where to find?
1	**21-01148**	2021	*Yersinia enterocolitica*	-	-	This study	-	Fig. S6G, H	-	Fig. S6J
2	**21-01228**	2021	*Yersinia enterocolitica*	-	-	This study	-	Fig. S6G, H	-	Fig. S6J
3	**21-01304**	2021	*Yersinia enterocolitica*	-	-	This study	-	Fig. S6G, H	-	Fig. S6J
4	**21-01362**	2021	*Yersinia enterocolitica*	-	-	This study	-	Fig. S6G, H	-	Fig. S6J
5	**21-00139**	2021	*Salmonella enterica* S. Typhimurium	-	-	This study	-	Fig. S6G, H	-	Fig. S6J
6	**21-00776**	2021	*Salmonella enterica* S. Typhimurium	-	-	This study	-	Fig. S6G, H	-	Fig. S6J
7	**21-01538**	2021	*Salmonella enterica* S. Enteritidis	-	-	This study	-	Fig. S6G, H	-	Fig. S6J
8	**21-01653**	2021	*Salmonella enterica* S. Virginia	-	-	This study	-	Fig. S6G, H	-	Fig. S6J
9	**21-01797**	2021	*Salmonella enterica* S. Infantis	-	-	This study	-	Fig. S6G, H	-	Fig. S6J
10	**21-02318**	2021	*Salmonella enterica* S. Enteritidis	-	-	This study	-	Fig. S6G, H	-	Fig. S6J

Table S4: *Shigella* strains used in the study (Ramming et al., xxx).

The species or serovar was determined using Whole Genome Analysis, classical serotyping or PCR-based serotyping (Lang et al., 2019). +, positive analysis test result; -, negative analysis test result.

	Strain no.	Year of isolation	Species or serovar	Stx1 subtype	Stx2 subtype	Reference	FRET assay supernatant	where to find?	Vero cell cytotoxicity assay	where to find?	Stx ELISA	where to find?
1	**99-06909**	1999	*Shigella dysenteriae*	stx1a	-	This study	+	Fig. S9A, B	+	Fig. S9C	+	Fig. S9D
2	**99-08842**	1999	*Shigella dysenteriae*	stx1a	-	This study	+	Fig. S9A, B	+	Fig. S9C	+	Fig. S9D
3	**00-02084**	2000	*Shigella dysenteriae*	stx1a	-	This study	+	Fig. S9A, B	+	Fig. S9C	+	Fig. S9D
4	**00-02085**	2000	*Shigella dysenteriae*	stx1a	-	This study	-	Fig. S9A, B	-	Fig. S9C	+	Fig. S9D
5	**02-08837**	2002	*Shigella dysenteriae*	stx1a	-	This study	-	Fig. S9A, B	-	Fig. S9C	-	Fig. S9D
6	**98-08694**	1998	*Shigella flexneri*	-	stx2a	This study	-	Fig. S9A, B	-	Fig. S9C	-	Fig. S9D
7	**99-05100**	1999	*Shigella flexneri*	-	stx2a	This study	-	Fig. S9A, B	-	Fig. S9C	+	Fig. S9D
8	**06-02974**	2006	*Shigella flexneri*	-	stx2a	This study	+	Fig. S9A, B	+	Fig. S9C	+	Fig. S9D
9	**12-00009**	2012	*Shigella flexneri*	-	stx2a	This study	+	Fig. S9A, B	+	Fig. S9C	+	Fig. S9D
10	**12-00266**	2012	*Shigella flexneri*	-	stx2a	This study	+	Fig. S9A, B	+	Fig. S9C	+	Fig. S9D
11	**21-00612**	2021	*Shigella flexneri*	-	stx2a	This study	-	Fig. S9A, B	-	Fig. S9C	-	Fig. S9D

Supplemental Methods

Western blot analysis. STEC culture supernatants or cell lysates were electrophoretically separated on a 15 % SDS-polyacrylamide gel. Proteins were transferred to a methanol (99.9 %, Carl Roth GmbH, Karlsruhe, Germany)-activated nitrocellulose membrane (Merck Millipore; Darmstadt, Germany). The membrane was then blocked in 5 % milk (in TBS-T, Sigma-Aldrich, Darmstadt, Germany) at 4 °C overnight. Primary monoclonal mouse antibodies against Stx1 (MBS5307327; MyBioSource Inc., San Diego, USA) or Stx2 (VT 135/6-B9; Sifin, Berlin, Germany) were added at a dilution of 1:1,000 for 3 h. StarBright Blue 520 Conjugated Goat Anti-Mouse Fluorescent Secondary Antibodies (Bio-Rad Laboratories; Feldkirchen, Germany) were used as secondary antibody at a dilution of 1:50,000 for 1 h. Stx was detected by fluorescence at 520 nm (ChemiDoc MP, Bio-Rad Laboratories, StarBright 520 channel).

Vero cell cytotoxicity assay. Toxicity of Stx towards Vero cells was determined as described previously (Roberts et al., 2001) with modifications. Prior to addition of culture supernatants, $1x10^5$ Vero cells/mL were seeded into a 96 well-plate (Greiner Bio-One; Kremsmünster, Austria) and were incubated for 24h at 37 °C and 5 % CO_2. Culture supernatants were diluted 1:400 in DMEM with 10 % FBS and 200 µL were added to each well and incubated for 48 h at 37 °C and under 5 % CO_2. After incubation, the cells were washed with 1× PBS and 100 µL 1-(4,5-Dimethylthiazol-2-yl)-3,5-diphenylformazan (MTT; 0.5 mg/mL in PBS; Sigma) were added for 1 h. After removal, 100 µL acidified isopropanol (isopropanol with 4 % v/v HCl, 32 %) were added. The absorption at 570 nm was photometrically measured at 570 nm (Tecan Infinite M-1000 Pro; Tecan, Suisse) (Mosmann, 1983). The proportion of damaged to viable cells (viability, in %) was calculated using mean absorbance of sample/mean absorbance of Vero cell control × 100.

References of supplemental data

Tab. S1, Fig. S1

Basu, D., Li, X. P., Kahn, J. N., May, K. L., Kahn, P. C., & Tumer, N. E. (2015). The A1 subunit of Shiga toxin 2 has higher affinity for ribosomes and higher catalytic activity than the A1 subunit of Shiga toxin 1. *Infection and Immunity*, *84*(1), 149–161. https://doi.org/10.1128/IAI.00994-15

Bergan, J., Dyve Lingelem, A. B., Simm, R., Skotland, T., & Sandvig, K. (2012). Shiga toxins. *Toxicon*, *60*(6), 1085–1107. https://doi.org/10.1016/j.toxicon.2012.07.016

Chan, Y. S., & Ng, T. B. (2016). Shiga toxins: from structure and mechanism to applications. *Applied Microbiology and Biotechnology*, *100*(4), 1597–1610. https://doi.org/10.1007/S00253-015-7236-3/TABLES/1

Gyles, C. L., De Grandis, S. A., MacKenzie, C., & Brunton, J. L. (1988). Cloning and nucleotide sequence analysis of the genes determining verocytotoxin production in a porcine edema disease isolate of Escherichia coli. *Microbial Pathogenesis*, *5*(6), 419–426. https://doi.org/10.1016/0882-4010(88)90003-4

Jackson, M. P. (1990). Mini-review Structure-function analyses of Shiga toxin and the Shiga-like toxins. *Microbial Pathogenesis*, *8*, 23–28.

Li, X. P., & Tumer, N. E. (2017). Differences in ribosome binding and sarcin/ricin loop depurination by shiga and ricin holotoxins. *Toxins*, *9*(4), 1–12. https://doi.org/10.3390/toxins9040133

Menge, C. (2020). Molecular biology of escherichia coli shiga toxins' effects on mammalian cells. In *Toxins* (Vol. 12, Issue 5). https://doi.org/10.3390/toxins12050345

Mosmann, T. (1983). Rapid colorimetric assay for cellular growth and survival: Application to proliferation and cytotoxicity assays. *Journal of Immunological Methods*, *65*(1–2), 55–63. https://doi.org/10.1016/0022-1759(83)90303-4

Roberts, P. H., Davis, K. C., Garstka, W. R., & Bhunia, A. K. (2001). Lactate dehydrogenase release assay from Vero cells to distinguish verotoxin producing Escherichia coli from non-verotoxin producing strains. *Journal of Microbiological Methods*, *43*(3), 171–181. https://doi.org/10.1016/S0167-7012(00)00222-0

Rocha, L. B., & Piazza, R. M. F. (2007). Production of Shiga toxin by Shiga toxin-expressing Escherichia coli (STEC) in broth media: From divergence to definition. *Letters in Applied Microbiology*, *45*(4), 411–417. https://doi.org/10.1111/j.1472-765X.2007.02214.x

Scheutz, F., Teel, L. D., Beutin, L., Piérard, D., Buvens, G., Karch, H., Mellmann, A., Caprioli, A., Tozzoli, R., Morabito, S., Strockbine, N. A., Melton-Celsa, A. R., Sanchez, M., Persson, S., & O'Brien, A. D. (2012). Multicenter evaluation of a sequence-based protocol for subtyping Shiga toxins and standardizing Stx nomenclature. *Journal of Clinical Microbiology*, *50*(9), 2951–2963. https://doi.org/10.1128/JCM.00860-12

Steyert, S. R., Sahl, J. W., Fraser, C. M., Teel, L. D., Scheutz, F., & Rasko, D. A. (2012). Comparative genomics and stx phage characterization of LEE-negative Shiga toxin-producing Escherichia coli. *Frontiers in Cellular and Infection Microbiology*, *2*, 133. https://doi.org/10.3389/FCIMB.2012.00133/BIBTEX

Takeda, Y., Kurazono, H., & Yamasaki, S. (1993). Minireview Vero Toxins (Shiga-Like Toxins) Produced by Enterohemorrhagic •ôNH•ôEscherichia coli•ôNS•ô (Verocytotoxin-Producing •ôNH•ôE. coil•ôNS•ô). *Microbiol. Immunol*, *37*(8), 591–599.

Yamasaki, S., Furutani, M., Ito, K., Igarashi, K., Nishibuchi, M., & Takeda, Y. (1991). Importance of

arginine at position 170 of the A subunit of Vero toxin 1 produced by enterohemorrhagic Escherichia coli for toxin activity. *Microbial Pathogenesis*, *11*(1), 1–9. https://doi.org/10.1016/0882-4010(91)90088-R

Yang, X., Liu, Q., Sun, H., Xiong, Y., Matussek, A., & Bai, X. (2022). Genomic Characterization of Escherichia coli O8 Strains Producing Shiga Toxin 2l Subtype. *Microorganisms*, *10*(6), 1245. https://doi.org/10.3390/microorganisms10061245

Supplemental Methods

Roberts, P. H., Davis, K. C., Garstka, W. R., & Bhunia, A. K. (2001). Lactate dehydrogenase release assay from Vero cells to distinguish verotoxin producing Escherichia coli from non-verotoxin producing strains. *Journal of Microbiological Methods*, *43*(3), 171–181. https://doi.org/10.1016/S0167-7012(00)00222-0

Tab. S2-S4 (Excel file with sub tables)

Frank, C., Werber, D., Cramer, J. P., Askar, M., Faber, M., an der Heiden, M., Bernard, H., Fruth, A., Prager, R., Spode, A., Wadl, M., Zoufaly, A., Jordan, S., Kemper, M. J., Follin, P., Müller, L., King, L. A., Rosner, B., Buchholz, U., … Krause, G. (2011). Epidemic Profile of Shiga-Toxin–Producing Escherichia coli O104:H4 Outbreak in Germany. *New England Journal of Medicine*, *365*(19), 1771–1780. https://doi.org/10.1056/NEJMOA1106483/SUPPL_FILE/NEJMOA1106483_DISCLOSURES.PDF

Gobert, A. P., Vareille, M., Glasser, A.-L., Hindré, T., De Sablet, T., & Martin, C. (2007). Shiga Toxin Produced by Enterohemorrhagic Escherichia coli Inhibits PI3K/NF-B Signaling Pathway in Globotriaosylceramide-3-Negative Human Intestinal Epithelial Cells 1. *The Journal of Immunology*, *178*, 8168–8174. http://journals.aai.org/jimmunol/article-pdf/178/12/8168/1231196/zim01207008168.pdf

Lang, C., Hiller, M., Konrad, R., Fruth, A., & Flieger, A. (2019). Whole-Genome-Based Public Health Surveillance of Less Common Shiga Toxin-Producing Escherichia coli Serovars and Untypeable Strains Identifies Four Novel O Genotypes. *Journal of Clinical Microbiology*, *57*(10). https://doi.org/10.1128/JCM.00768-19

Lang, C., Fruth, A., Campbell, I. W., Jenkins, C., Smith, P., Weill, F.-X., Nübel, U., Grad, Y. H., & Flieger, A. (2023). O-antigen diversification masks identification of highly pathogenic STEC O104:H4-like 1 strains 2 3. *Microbiology Spectrum*. https://doi.org/10.1101/2022.09.15.508078

Perna, N. T., Plunkett, G., Burland, V., Mau, B., Glasner, J. D., Rose, D. J., Mayhew, G. F., Evans, P. S., Gregor, J., Kirkpatrick, H. A., Pósfai, G., Hackett, J., Klink, S., Boutin, A., Shao, Y., Miller, L., Grotbeck, E. J., Davis, N. W., Lim, A., Blattner, F. R. (2001). Genome sequence of enterohaemorrhagic Escherichia coli O157:H7. *Nature*, *409*(6819), 529–533. https://doi.org/10.1038/35054089

Schmidt, H., Russmann, H., & Karch, H. (1993). Virulence determinants in nontoxinogenic Escherichia coli O157 strains that cause infantile diarrhea. *Infection and Immunity*, *61*(11), 4894–4898. https://doi.org/10.1128/IAI.61.11.4894-4898.1993